

Fluorescent turn-on detection of cysteine using a molecularly imprinted polyacrylate linked to allylthiol-capped CdTe quantum dots

Mu-Rong Chao · Chiung-Wen Hu · Jian-Lian Chen

Received: 15 December 2013 / Accepted: 13 February 2014 / Published online: 11 March 2014
© Springer-Verlag Wien 2014

Abstract CdTe quantum dots capped with thioglycolic acid (TGA) display a strong turn-on fluorescence response if exposed to solutions of cysteine (Cys). In order to exploit this effect, a molecularly imprinted polymer (MIP) for Cys was covalently linked to the QDs via allyl mercaptan. The resulting nanomaterials (QDs, MIP-coated QDs, and nonimprint-coated QDs) were characterized by FTIR and scanning electron microscopy. The adsorption of Cys was studied in phosphate buffer (pH 7.4) with respect to equilibration times (5, 15, and 40 min, respectively), binding constants [2.98, 2.42, and 0.96 ($\times 10^4 \text{ M}^{-1}$)], and Langmuir isotherms ($R^2=0.9995, 0.9999,$ and 0.9983) in the Cys concentration range between $3.33 \mu\text{M}$ to $500 \mu\text{M}$. The method has a detection limit of $0.85 \mu\text{M}$ (3σ , blank, for $n=10$). The selectivity of the MIP-coated QDs for Cys over 19 other amino acids is similar to that of bare QDs, but MIP-QDs afford better recoveries of Cys from solutions

also containing bovine serum albumin (90 %) and fetal bovine serum (97 %), respectively, when compared to the recoveries that are obtained with bare (non-imprinted) QDs (135 % and 120 %). This is probably due to the fact that the outer MIP shell largely reduces protein wrapping, dot aggregation, and matrix inclusion.

Keywords Cysteine · Fluorescence · Molecularly imprinted polymer · CdTe nanocrystal · Polyacrylate · Quantum dot

Introduction

Many quantum dots (QDs), which are most often composed of metal chalcogenides and their derivatives, have been used as fluorescence probes to detect ions, molecules, proteins, enzymes, and cells [1–4]. The effective recognition of target constituents in a variable biomatrix is the key to developing successful QD probes and is usually achieved using receptor-specific molecules as the recognition materials coupled to QD surfaces, such as ion-selective ligands [5], ionophores [6], cyclodextrins [7], dendrimers [8], and biomolecules, including enzymes [9], antibodies [1], and aptamers [10].

Molecular imprinting also creates a receptor-specific polymeric network with specific three-dimensional recognition and binding sites that are complementary to the template analyte [11]. In contrast to bulk monoliths, molecularly imprinted polymers (MIP) on nanoparticles have higher surface area-to-volume ratios and thus the imprinted cavities are more easily accessible by templates and the binding kinetics is improved [12]. Composites of MIPs and chalcogenide QDs have been successfully applied as sensing materials for molecular and biomolecular Templates. A biocompatible polymer, poly(ethylene-co-ethylene alcohol), was used to couple QDs and biotemplates with the phase inversion method [13]. Additionally, a sol-gel technique was utilized in MIP-QD

Electronic supplementary material The online version of this article (doi:10.1007/s00604-014-1209-6) contains supplementary material, which is available to authorized users.

J.-L. Chen (✉)

School of Pharmacy, China Medical University, No. 91 Hsueh-Shih Road, Taichung 40402, Taiwan
e-mail: cjl@mail.cmu.edu.tw

M.-R. Chao

Department of Occupational Safety and Health, Chung Shan Medical University, Taichung 402, Taiwan

M.-R. Chao

Department of Occupational Medicine, Chung Shan Medical University Hospital, Taichung 402, Taiwan

C.-W. Hu

Department of Public Health, Chung Shan Medical University, Taichung 402, Taiwan

C.-W. Hu

Department of Family and Community Medicine, Chung Shan Medical University Hospital, Taichung 402, Taiwan

fabrication for the optosensing of phenols [14], pyrethroids [15], ractopamine [16], and proteins [17].

In contrast, organic polymer-based MIPs conjugated with QDs have also been developed for optosensing small molecules [18–21] and DNA [22] by a fluorescence quenching mechanism. These MIPs were mainly synthesized via in situ polymerization of an ethylene glycol dimethacrylate crosslinker and methacrylic acid as the functional monomer. Unlike the role that the functional monomer plays in the sol-gel process, methacrylic acid, which lacks the ability to strongly donate electrons to QDs, is unable to conjugate QDs and MIPs, although it can assist in forming imprinted cavities. Before in situ polymerization with MIP monomers, QDs have previously been functionalized with an anchor, such as 4-vinylpyridine [18], 1-vinyl-3-octylimidazolium [20], or methacryloylamidocysteine [22], to strengthen the electron donation. An alternative method that has been used is to activate the carboxylic acid side groups of the MIP monoliths in advance to allow chemical attachment to commercially available amine-functionalized QDs [19]. In particular, a composite of polystyrene-co-methacrylic acid MIPs and QDs has been synthesized without the addition of crosslinker or the functionalization of QDs [21].

In this study, a small and simple molecule, allylthiol, was first used to establish a link between the CdTe QDs and MIP acrylate monomers. After characterization by FTIR, SEM, and fluorophotometry, the MIP-QD composite, a product of one-pot polymerization, was capable of fluorescent turn-on sensing of cysteine in bovine serum albumin- and fetal bovine serum-containing media and its sensing ability was compared to that of the bare QDs and non-imprinted polymer (NIP) modified QDs via kinetic and thermodynamic data.

Experimental

Materials and chemicals

$\text{CdCl}_2 \cdot 2.5\text{H}_2\text{O}$, tellurium powder, NaBH_4 , thioglycolic acid (TGA), ethanol, and phosphate salts were purchased from Acros (Thermo Fisher Scientific, Geel, Belgium; <http://www.acros.com>). Allyl mercaptan (AM) and methacrylic acid (MAA) were purchased from Alfa Aesar (Ward Hill, MA; <http://www.alfa.com>). The ethylene glycol dimethacrylate (EGDMA), α, α' -azobisisobutyronitrile (AIBN), 1-propanol, 1,4-butanediol, and hydrophilic ionic liquid 1-ethyl-3-methylimidazolium dicyanamide were purchased from Aldrich (Milwaukee, WI, USA; <http://www.sigmaaldrich.com>). Bovine serum albumin (lyophilized powder, mol. wt. ~ 66 kDa) and fetal bovine serum (hemoglobin ≤ 25 $\text{mg} \cdot \text{dL}^{-1}$) were purchased from Sigma (Milwaukee, WI, USA; <http://www.sigmaaldrich.com>).

The 20 amino acids were purchased from TCI (Asp and Ala) (Tokyo, Japan; <http://www.tcichemicals.com>), MP

Biomedicals (Asn, Val, and Leu) (Eschwege, Germany; <http://www.mpbio.com>), Alfa Aesar (Glu, Lys, Arg, Pro, Ile, Tyr, and His), Sigma (Gln, Ser, and Trp), and Acros (Thr, Met, Cys, Gly, and Phe). The other test solutes were purchased from Acros (uric acid), Alfa Aesar (caffeine), and Aldrich (citric acid, glucose, ascorbic acid, and bis(2-ethylhexyl)phthalate). Purified water (18 $\text{M}\Omega\text{-cm}$) from a Milli-Q water purification system (Millipore, Bedford, MA, USA) was used to prepare the standard salt and buffer solutions. All standard solutions were protected from light and kept at 4 °C in a refrigerator.

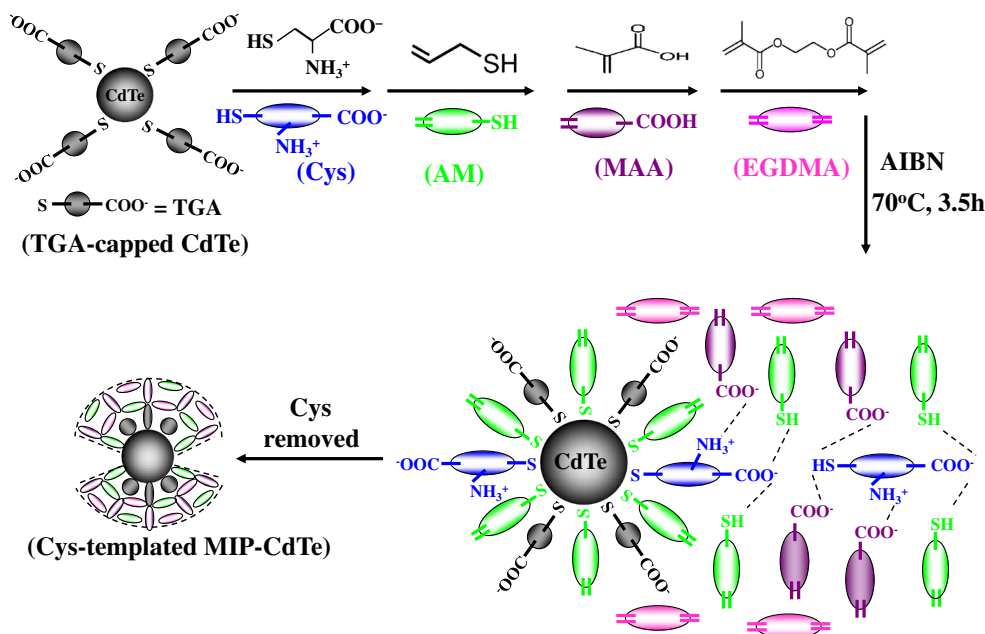
Synthesis and characterization of the polymer-quantum dot composites

The synthesis of thioglycolic acid-capped CdTe (TGA-CdTe) followed the previously published method [23]. In brief, an aqueous solution of NaHTe , prepared by the reduction of tellurium powder with excess NaBH_4 in water with stirring and under N_2 , was injected into an aqueous TGA- CdCl_2 solution. Solutions were deaerated with N_2 for 20 min. Subsequently, a mixture of $\text{Cd}^{2+}/\text{HTe}^-/\text{TGA}$, at a molar ratio of 1 : 0.5 : 2.4, was heated at 100 °C for 8 h. After heating, the hydrophilic TGA-CdTe QDs were formed in the aqueous solution and used as the base QDs for the subsequent preparation of MIP-QDs and NIPs.

The Cys-templated MIP-QD was prepared by first preparing a reagent cocktail that was obtained by sequential addition of 60.6 mg of Cys, 223 mg of allyl mercaptan, 86.1 mg methacrylic acid, 198 mg ethylene glycol dimethacrylate, 2.0 mL of a 1:1 mixture of 1-propanol and 1,4-butanediol, and 0.5 mL of a saturated solution of α, α' -azobisisobutyronitrile in a 1:1:1 mixture of 1-propanol, 1,4-butanediol, and water to 0.5 mL of a QD solution containing 625 mg of QDs. The reagent cocktail was then heated at 70 °C for 3.5 h to complete the one-pot polymerization. The polymerization products (Cys-MIP-QDs) containing adsorbed Cys templates were filtered from the mixture and successively washed with 80 mL of ethanol/water (3/1, v/v) to obtain the Cys-free MIP-QDs (MIP-QDs). The scheme of the preparation process is illustrated in Fig. 1. NIPs were obtained by following the same procedure as described for the preparation of the MIP-QDs, except without the addition of Cys to the bare QD solution. After washing thoroughly and drying in an oven at 40 °C for 30 min, the MIP-QD and NIP samples were ready to be characterized by FTIR (Prestige-21, Shimadzu) and scanning electron microscopy (SEM; JSM-6700F, JOEL) at an accelerating voltage of 3.0 kV.

Three additional materials were synthesized in the same manner and using the same ratio of components. First, TGA-CdTe was replaced with hydrophilic ionic liquid (IL)-passivated CdTe nanocrystals (NC_{IL}), the synthesis of which followed the previously published method [23], to form MIP- NC_{IL} . Second, an allyl mercaptan-free MIP-QD composite was synthesized

Fig. 1 Scheme for the preparation of MIP-coated CdTe quantum dots. TGA: thioglycolic acid; AM: allyl mercaptan; MAA: methacrylic acid; EGDMA: ethylene glycol dimethacrylate; Cys: cysteine; AIBN: α, α' -azobisisobutyronitrile



without the addition of allyl mercaptan. Third, a QD- and Cys-free polymer (allyl mercaptan-methacrylic acid-ethylene glycol dimethacrylate) was prepared using a monomer mixture containing only allyl mercaptan, methacrylic acid, and ethylene glycol dimethacrylate. However, the materials were dispersed in the reaction solvent and were not able to be separated by filtration. Their detailed discussion is supplemented in [Electronic Supplementary Material](#) (ESM).

Spectrofluorimetric determination of cysteine

Fluorescence spectra, using excitation at 315 nm, were collected with a spectrofluorophotometer (LS55, Perkin Elmer) from various samples to which the QD probe had been added, either 1 μL of bare QDs ($1.25 \text{ g} \cdot \text{mL}^{-1}$), 1.25 mg of MIP-QDs, or 1.25 mg of NIPs, into 3.0 mL of phosphate buffer (pH 7.5, 50 mM) containing 0.33 mM of test solutes, including serum molecules and 20 amino acids. Bovine serum albumin (1.2 mg; 6 μM) or fetal bovine serum (0.15 mL; 5 %) were added to the phosphate buffer to verify the effect of the matrix on the QD probes. Fluorescence intensities were recorded at 540 nm.

Results and discussion

Selection of a potential template

In general, a suitable template should have a distinct fluorescence response to QDs and form imprinting cavities, which are appropriate for removing the bound template from the MIP-QD product in the washing step and for rebinding the free template to the washed product during the analytical step. It is important to identify the fluorescent performances of the

QD probes to templates or analytes of interest before proceeding to the fabrication of the MIP-QD composites. If the fluorescence sensitivity of a QD probe to a template is confirmed, the successful detection of the template by the MIP-QD probe is feasible.

In this study, serum molecule candidates were screened using the homogeneous fluorescence sensing platform composed of water-soluble TGA-CdTe, which had successfully been used as a QD probe for metal ions [24], nitrogen-containing heterocycles [25], antioxidants [26], surfactants [27], and radicals [28] by quenching fluorometry. As shown in Fig. S-1 (ESM), Cys and uric acid caused more distinct changes in the fluorescence intensity of the sensing platform in pH 7.4 phosphate buffers than the other molecules tested under the same conditions. Accordingly, MIP-QD adducts, templated with Cys and uric acid, were fabricated by following the scheme in Fig. 1. Although an excess of wash solvent and Soxhlet extraction time were attempted to release trapped uric acid from the templated cavity of the MIP-QD composite, the resulting fluorescence was still weak and unaltered. Unlike the failure of uric acid in the fabrication of uric acid-templated MIP-QDs, Cys-templated MIP-QD fabrication was successful. Thus, we characterized and investigated the potential application of this MIP-QD in fluorescence sensing.

Characterization of cysteine-templated molecular imprinted polymer-quantum dots

The synthesized Cys-templated MIP-QDs were characterized by FTIR, SEM, and spectrofluorometry. FTIR spectra of AM-MAA-EGDMA copolymer, NIPs, MIP-QDs, and bare QDs are shown in Fig. S-2 (ESM). The comparison of absorption peaks between the spectra was discussed in [Electronic](#)

supplementary material. Overall, the spectra of NIPs and MIP-QDs both possessed the characteristic peaks of the allyl mercaptan-methacrylic acid-ethylene glycol dimethacrylate copolymer and TGA-CdTe, and the two spectra were barely distinguishable.

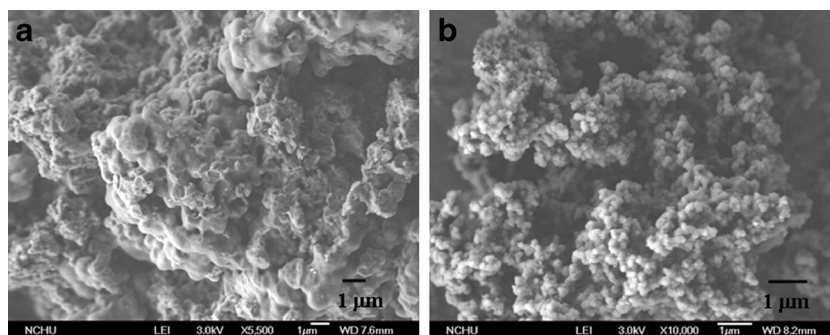
The SEM images of NIP and MIP-QD morphology depicted in Fig. 2 were distinguishable. As shown in the images, the polyacrylate layers heavily coated the NIP particles and filled the spaces between them. The granular diameter size for the entangled NIP particles was nearly ten times larger than for the MIP-QDs (1.0 μm vs. 0.1 μm). The Cys templates competed with the alkenyl monomers to be adsorbed onto the CdTe particle surfaces and impeded the propagation growth of the polyacrylate chain. This resulted in the formation of smaller and more uniform MIP-QD particles.

The fluorescence spectra of NIPs, MIP-QDs (after removing Cys by washing), and Cys-MIP-QDs (before removing Cys by washing) are presented in Fig. 3a, b and j, respectively, and show the successive increase in their PL intensities. Furthermore, the PL intensities of the polymer-modified QDs in the fabrication process have remarkable reproducibility, both within and between batches ($\sigma < 3.0\%$, $n = 20$, five samples for each of four batches). Wang et al. reported that the addition of Cys led to an increase of the PL intensity of TGA-CdTe as a result of passivation of Cd^{2+} defects on the surfaces of QDs by the coordination of thiol groups in Cys molecules [29]. Therefore, stripping Cys from MIP-QDs decreased the PL intensity. The lower intensity observed for NIPs was mainly due to the heavier polyacrylate layers on the NIP particles than on MIP-QDs, as shown in the SEM images in Fig. 2. Thus the number of CdTe particles per unit weight of NIPs was less than for MIP-QDs.

Fluorescent sensing of cysteine by cysteine-templated molecular imprinted polymer-quantum dots

Cys-templated MIP-QDs were prepared and used as a homogeneous fluorescence-sensing platform, in which response time, dosage, and specificity for Cys molecules were studied in sequence.

Fig. 2 Scanning electron microscope images of **a** NIPs, and **b** MIP-QDs



Time response

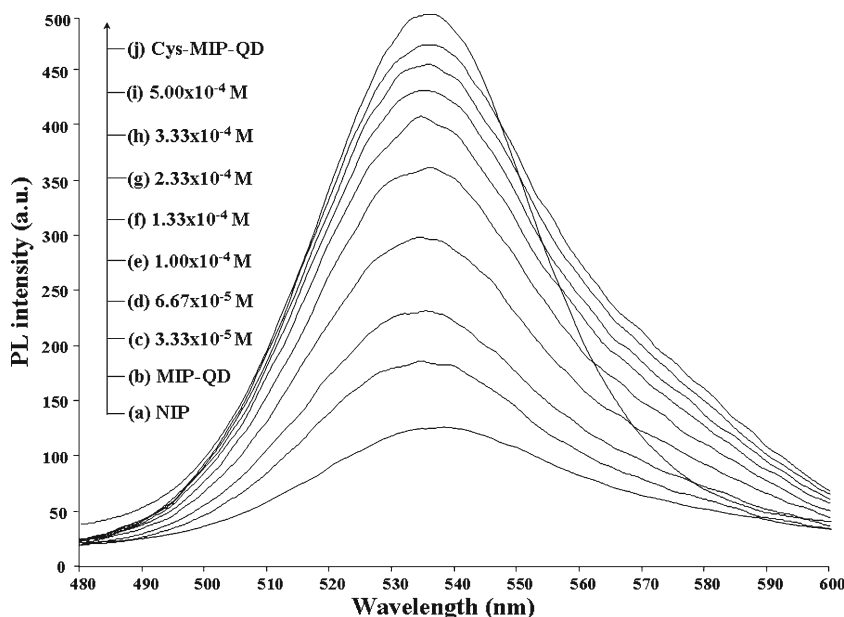
After exposing the QD probes ($0.42 \text{ mg} \cdot \text{mL}^{-1}$) to the Cys analyte (0.33 mM), a plot of PL intensity versus response time was recorded and is shown in Fig. 4. This plot revealed that the coordination of Cys with MIP-QDs reached equilibrium at approximately 15 min after the addition of Cys in pH 7.4 phosphate buffer. After 15 min, the increase in PL intensity was less than 3.0 % RSD. As shown in the SEM images in Fig. 2, the heavy coating of polyacrylate blocked most of paths for the Cys molecules diffusing to exterior binding sites on the NIP surface or through cavity channels to the interior binding sites embedded in the NIP and decreased the fluorescent core numbers per unit weight of NIP. Accordingly, for NIPs, a distinct increase in PL intensity was not observed after 40 min and reaching equilibrium required longer than 40 min. Without any polymer shielding, the bare QDs displayed the shortest equilibrium time (5 min) and the highest increase in PL intensity.

Dose response

The PL intensities of each probe, including the bare QDs, Cys-MIP-QDs, MIP-QDs, and NIPs, were measured after equilibrium with Cys molecules in pH 7.4 phosphate buffer and plotted against the Cys concentrations used in Fig. S-3(a) (ESM). As shown in Fig. S-3(a), the PL intensities increased with the concentration of Cys as expected and finally reached plateaus in a decreasing order as follows: bare QD > Cys-MIP-QD \approx MIP-QD > NIP. A high plateau is correlated with the presence of numerous binding sites or templated cavities conjugated with Cys. When the plateau levels were compared with the time responses for the QD probes, it was found that the shorter the equilibrium time, the sharper the increase in PL intensity was. That is, the binding sites on the bare QDs were plentiful and accessible to Cys molecules, but those on the NIPs were not.

The response of MIP-QDs to Cys was moderate. Additionally, the fluorescence spectra of MIP-QDs measured at different concentrations of Cys, $3.33 \times 10^{-5} \text{ M} \sim 5.00 \times 10^{-4} \text{ M}$, are shown in Fig. 3c~i. At high concentrations of Cys, the PL intensities of MIP-QDs were very close to those of Cys-MIP-QDs, as shown in Fig. S-3(a). This indicated that the templated cavities available for both composites were nearly equal in quantity and

Fig. 3 Fluorescence spectra ($\lambda_{\text{ex}}=315$ nm) of the modified QD solutions ($0.42 \text{ mg}\cdot\text{mL}^{-1}$) of **a** NIPs, **b** MIP-QDs, **c~i** MIP-QDs with addition of the indicated concentrations of cysteine, and **j** cysteine-MIP-QDs



stayed active upon the kinetic sorption/desorption of Cys with the QD probes. This reversible process could be further described by a Langmuir isotherm, which assumes that there is a finite number of binding sites distributed homogeneously over the adsorbent surfaces and that each of them can adsorb one Cys target molecule from solution. With such assumptions, the Langmuir description that relates the Cys concentration, C , to the PL intensity, I , can be written as [30]

$$C/I = 1/(BI_{\text{max}}) + (1/I_{\text{max}})C$$

where the binding constant B , defined as the ratio of the sorption and desorption rate constants, and the maximum intensity I_{max} were obtained from the linearized Langmuir equation by plotting C/I versus C . As shown in Fig. S-3(b), B ($2.98, 2.42,$ and $0.96 \times 10^4 \text{ M}^{-1}$) and I_{max} ($1,280, 502,$ and 260 a.u.) for the bare QDs, MIP-QDs, and NIPs were calculated based on the high linearities of $R^2=0.9995, 0.9999,$ and 0.9983 , respectively, in a concentration range of Cys from

$3.33 \mu\text{M}$ to $500 \mu\text{M}$. A detection limit of $0.55 \mu\text{M}$ and $0.85 \mu\text{M}$ was determined respectively by the bare QDs and MIP-QDs solution without Cys ($3\sigma, n=10$). The high B value for the bare QDs was mainly due to ample available space allowing Cys to be exothermically adsorbed in a valid direction around the binding sites, although ample space also favored the free desorption of Cys from binding sites. The space of the templated cavities formed in MIP-QDs was more confined than in the non-polymer-coated bare QDs but more spacious than in the non-templated NIPs, which contained tangled polyacrylate. Therefore, the B value for MIP-QDs was lower than for bare QDs but higher than for NIPs. In addition, the B values also revealed the fraction of occupied active sites in equilibrium with a given concentration of target molecule. Here the difference in the fractions of occupied sites between the QD probes ($50 \%, 44 \%,$ and 24% , respectively) equilibrated with $3.3 \times 10^{-5} \text{ M}$ Cys was larger than when they were equilibrated with $1.3 \times 10^{-3} \text{ M}$ Cys ($98 \%, 97 \%,$ and 93% , respectively). The I_{max} values, which are proportional to the maximum number of valid binding sites and the thermodynamic stability of the sites associated with targets, correlated well with the plateau levels shown in Fig. S-3(a) (ESM).

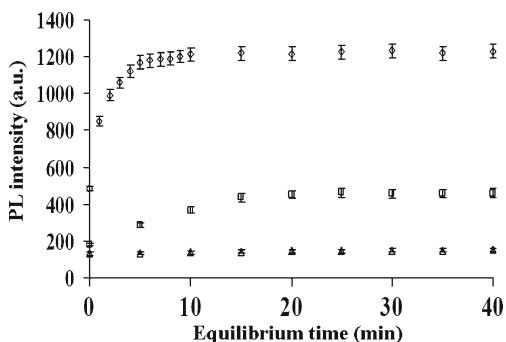


Fig. 4 Study of kinetic binding of cysteine (0.33 mM) onto the different QD probes ($0.42 \text{ mg}\cdot\text{mL}^{-1}$) with PL detection ($\lambda_{\text{ex}}=315$ nm, $\lambda_{\text{em}}=540$ nm). (white diamond) bare QDs, (white square) MIP-QDs, and (white triangle) NIPs

Specificity study

Among the molecules tested in Fig. S-1, Cys apparently increased the PL intensity because of its ability to passivate the defects on bare QD surfaces. Other amino acids were also tested with bare QD, MIP-QD, and NIP solutions under the same conditions as in Fig. S-1 (ESM). As shown in Fig. S-4 (ESM), the results indicate that the changes in PL intensity are only observed in the bare QDs or MIP-QDs when probing for Cys. Although the MIP-QDs had a higher specificity for Cys

Table 1 Comparable methods for the fluorimetric determination of cysteine with quantum dots

Materials used	Analytical ranges; μM (LOD; nM)	Interferents studied	Sample matrices	Comments	Reference
Mercaptoacetic acid capped CdSe/ZnS	0.01~0.8 (3.8)	Amino acids, ions, carbohydrates, nucleotide acids	Treated human urine	Easy preparation for QD materials; complex buffers containing NaCl and Triton X-100	[32]
Citrate capped CdS	0.01~50 (5.4)	Amino acids, ions, carbohydrates	Treated human urine	Easy preparation for QD materials; basic for biological fluid samples conditioned at pH 9.0	[33]
Citrate capped CdS	0.01~5 (3.3)	Amino acids	Treated human serum	Easy preparation for QD materials; acidic for biological fluid samples conditioned at pH 2.87	[34]
Phenanthroline on thioglycolic acid capped CdTe/CdS	1~70 (780)	Amino acids, proteins, metal ions, carbohydrates, nucleotides, thiols	Treated human serum	Selectivity enhancement with the exclusion of interferents from the phenanthroline surrounding QD core; reduced sensitivity	[35]
MIP on thioglycolic acid capped CdTe	3~500 (850)	Amino acids	Bovine serum albumin; fetal bovine serum	Selectivity enhanced by the MIP shield against interferents; changeable imprinted molecule; preparation with steps; reduced sensitivity	this study

over the other amino acids than NIPs, the superiority of MIP-QDs over bare QDs was questionable. The function of MIP coating on the MIP-QDs was not confirmed in the simple phosphate buffer. However, the addition of a protein matrix, such as bovine serum albumin or fetal bovine serum, to the Cys solutions could approximate the complexity of real world samples and further test MIP function.

As shown in Fig. S-5 (ESM), the ratios of PL intensity, defined as a percentage recovery and measured in the presence of protein matrix over that without protein matrix in the same phosphate buffer, were plotted against equilibrium time. For bare TGA-CdTe QDs, the recoveries of Cys from spiked bovine serum albumin and fetal bovine serum were approximately 135 % ($n=6$, R.S.D.=11.8 %) and 120 % ($n=6$, R.S.D.=14.5 %), respectively, at 60 min and deviated from the ideal 100 %. According to Podery's report [31], the high recovery from bovine serum albumin is due to the formation of a bovine serum albumin coating on the bare QD surface, which prevents aggregation of QDs and the rapid washout of the TGA passivant. In this study, the formation of a fetal bovine serum coating and its preventative effects were somewhat less efficient and thus Cys recovery was lower than recovery in bovine serum albumin. For the MIP-QDs, which presented the optimal recoveries of 90 % from bovine serum albumin ($n=6$, R.S.D.=3.4 %) and 97 % from fetal bovine serum ($n=6$, R.S.D.=4.8 %), the outer MIP shell largely reduced protein wrapping, QD aggregation, and matrix inclusion. With the merits of MIP selectivity and changeable target template, MIP-QDs were comparable to the other QD materials used for the fluorimetric determination of Cys, although their preparation took more steps and reduced the sensitivity (Table 1). The protein matrices can interact with Cys

analytes and interrupt those entering the binding sites, which may lead to lower recoveries. In addition, protein matrices may directly interact with the surface sites and affect QD passivation and PL intensity. Each of these factors contributed to the final recoveries. For NIPs, most of accessible binding sites were on the surface. The recoveries of 86 % from bovine serum albumin ($n=6$, R.S.D.=10.3 %) and 75 % from fetal bovine serum ($n=6$, R.S.D.=12.7 %) were obviously greatly affected by the protein matrices, especially fetal bovine serum, which contains many small molecules.

Conclusion

A small and simple molecule, allyl mercaptan, was designed to couple polyacrylate MIPs and TGA-CdTe QDs. Cys was selected as an MIP template because of high increase in PL intensity upon its binding with QDs. The Cys-templated MIP-conjugated QDs prepared via a one-pot polymerization were successfully characterized by FTIR, SEM, and fluorometry. The equilibrium time required for Cys to diffuse toward the QD probes, including bare QDs, Cys-templated MIP-QDs, and non-Cys-templated NIP-QDs, were 5, 15, and 40 min, respectively. Based on Langmuir isotherms ($R^2=0.9995$, 0.9999, and 0.9983) in a concentration range of Cys from 3.33 μM to 500 μM , the binding constants (2.98, 2.42, and 0.96 ($\times 10^4 \text{ M}^{-1}$)) for the QD probes were obtained. With the outer MIP shell, which prevented protein wrapping, QD aggregation, and matrix inclusion, MIP-QDs showed better recoveries of Cys from bovine serum albumin (90 %) and fetal bovine serum (97 %) than bare QDs (135 % and 120 %).

Acknowledgments Support for this work by the National Science Council of Taiwan under Grant no. NSC-101-2113-M-039-001-MY3 and the China Medical University under Grant no. CMU101-S-11 is gratefully acknowledged.

References

1. Esteve-Turrillas FA, Abad-Fuentes A (2013) Applications of quantum dots as probes in immunosensing of small-sized analytes. *Biosens Bioelectron* 41:12–29
2. Kuang H, Zhao Y, Ma W, Xu L, Wang L, Xu C (2011) Recent developments in analytical applications of quantum dots. *Trends Anal Chem* 30:1620–1636
3. Delehanty JB, Susumu K, Manthe RL, Algar WR, Medintz IL (2012) Active cellular sensing with quantum dots: transitioning from research tool to reality; a review. *Anal Chim Acta* 750:63–81
4. Ruedas-Rama MJ, Walters JD, Orte A, Hall EAH (2012) Fluorescent nanoparticles for intracellular sensing: a review. *Anal Chim Acta* 751:1–23
5. Li H, Han C, Zhang L (2008) Synthesis of cadmium selenide quantum dots modified with thiourea type ligands as fluorescent probes for iodide ions. *J Mater Chem* 18:4543–4548
6. Ruedas-Rama MJ, Hall EAH (2008) Azamacrocyclic activated quantum dot for zinc ion detection. *Anal Chem* 80:8260–8268
7. Aguilera-Sigalat J, Casas-Solvas JM, Morant-Miñana MC, Vargas-Berenguel A, Galian RE, Pérez-Prieto J (2012) Quantum dot/cyclodextrin supramolecular systems based on efficient molecular recognition and their use for sensing. *Chem Commun* 48:2573–2575
8. Algarra M, Campos BB, Alonso B, Miranda MS, Martínez ÁM, Casado CM, Esteves da Silva JCG (2012) Thiolated DAB dendrimers and CdSe quantum dots nanocomposites for Cd (II) or Pb (II) sensing. *Talanta* 88:403–407
9. Li DW, Qin LX, Li Y, Nia RP, Long YT, Chen HY (2011) CdSe/ZnS quantum dot–cytochrome c bioconjugates for selective intracellular O_2^- sensing. *Chem Commun* 47:8539–8541
10. Yuan Q, Lu D, Zhang X, Chen Z, Tan W (2012) Aptamer-conjugated optical nanomaterials for bioanalysis. *Trends Anal Chem* 39:72–86
11. Wulff G (2013) Forty years of molecular imprinting in synthetic polymers: origin, features and perspectives. *Microchim Acta* 180:1359–1370
12. Poma A, Tumer APF, Piletsky SA (2010) Advances in the manufacture of MIP nanoparticles. *Trends Biotechnol* 28:629–637
13. Lee MH, Chen YC, Ho MH, Lin HY (2010) Optical recognition of salivary proteins by use of molecularly imprinted poly (ethylene-co-vinyl alcohol)/quantum dot composite nanoparticles. *Anal Bioanal Chem* 397:1457–1466
14. Wang HF, He Y, Ji TR, Yan XP (2009) Surface molecular imprinting on Mn-doped ZnS quantum dots for room-temperature phosphorescence optosensing of pentachlorophenol in water. *Anal Chem* 81:1615–1621
15. Ge S, Lu J, Ge L, Yan M, Yu J (2011) Development of a novel deltamethrin sensor based on molecularly imprinted silica nanoparticles embedded CdTe quantum dots. *Spectrochim Acta A Mol Biomol Spectrosc* 79:1704–1709
16. Liu H, Liu D, Fang G, Liu F, Liu C, Yang Y, Wang S (2013) A novel dual-function molecularly imprinted polymer on CdTe/ZnS quantum dots for highly selective and sensitive determination of ractopamine. *Anal Chim Acta* 762:76–82
17. Zhang W, He XW, Chen Y, Li WY, Zhang YK (2012) Molecularly imprinted polymer anchored on the surface of denatured bovine serum albumin modified CdTe quantum dots as fluorescent artificial receptor for recognition of target protein. *Biosens Bioelectron* 31:84–89
18. Lin CI, Joseph AK, Chang CK, Lee YD (2004) Molecularly imprinted polymeric film on semiconductor nanoparticles: analyte detection by quantum dot photoluminescence. *J Chromatogr A* 1027:259–262
19. Stringer RC, Gangopadhyay S, Grant SA (2010) Detection of nitroaromatic explosives using a fluorescent-labeled imprinted polymer. *Anal Chem* 82:4015–4019
20. Liu H, Fang G, Li C, Pan M, Liu C, Fan C, Wang S (2012) Molecularly imprinted polymer on ionic liquid-modified CdSe/ZnS quantum dots for the highly selective and sensitive optosensing of tocopherol. *J Mater Chem* 19882–19887
21. Zhao Y, Ma Y, Li H, Wang L (2012) Correction to composite QDs@MIP nanospheres for specific recognition and direct fluorescent quantification of pesticides in aqueous media. *Anal Chem* 84:386–395
22. Diltemiz SE, Say R, Büyüktiryaki S, Hür D, Denizli A, Ersöz A (2008) Quantum dot nanocrystals having guanosine imprinted nanoshell for DNA recognition. *Talanta* 75:890–896
23. Chao MR, Chang YZ, Chen JL (2013) Hydrophilic ionic liquid-passivated CdTe quantum dots for mercury ion detection. *Biosens Bioelectron* 42:397–402
24. Zhong W, Zhang C, Gao Q, Li H (2012) Highly sensitive detection of lead (II) ion using multicolor CdTe quantum dots. *Microchim Acta* 176:101–107
25. Keane PM, Gallagher SA, Magno LM, Leising MJ, Clark IP, Greetham GM, Towrie M, Guíko YK, Kelly JM, Quinn SJ (2012) Photophysical studies of CdTe quantum dots in the presence of a zinc cationic porphyrin. *Dalton Trans* 41:13159–13166
26. Jhonsi MA, Vaishnavi E, Suganya R, Kathiravan A, Renganathan R (2011) Investigation on the photoinduced interaction between water soluble CdTe quantum dots and certain antioxidants. *Adv Sci Lett* 4:3490–3495
27. Diao XL, Xia YS, Zhang TL, Li Y, Zhu CQ (2007) Fluorescence-detecting cationic surfactants using luminescent CdTe quantum dots as probes. *Anal Bioanal Chem* 388:1191–1197
28. Adegoke O, Nyokong T (2012) A comparative study on the sensitive detection of hydroxyl radical using thiol-capped CdTe and CdTe/ZnS quantum dots. *J Fluoresc* 22:1513–1519
29. Wang Y, Zheng J, Zheng Z, Yuan C, Fu D (2009) CdTe nanocrystals as luminescent probes for detecting ATP, folic acid and l-cysteine in aqueous solution. *Colloids Surf A Physicochem Eng Asp* 342:102–106
30. Chen Y, Rosenzweig Z (2002) Luminescent CdS quantum dots as selective ion probes. *Anal Chem* 74:5132–5138
31. Poderys V, Matulionyte M, Selskis A, Rotomskis R (2011) Interaction of water-soluble CdTe quantum dots with bovine serum albumin. *Nanoscale Res Lett* 6:9
32. Huang S, Xiaoa Q, Li R, Guana HL, Liua J, Liu XR, Hea ZK, Liu Y (2009) A simple and sensitive method for l-cysteine detection based on the fluorescence intensity increment of quantum dots. *Anal Chim Acta* 645:73–78
33. Wanga GL, Donga YM, Yang HX, Li ZJ (2011) Ultrasensitive cysteine sensing using citrate-capped CdS quantum dots. *Talanta* 83:943–947
34. Chen S, Fan Y, Yang Y, Ye LY, Long YF (2012) Determination of cysteine based on fluorescence enhancement of CdS quantum dots with Cd^{2+} rich surface. *Chin J Anal Chem* 40:173–176
35. Chen S, Tian J, Jiang Y, Zhao Y, Zhang J, Zhao S (2013) A one-step selective fluorescence turn-on detection of cysteine and homocysteine based on a facile CdTe/CdS quantum dots–phenanthroline system. *Anal Chim Acta* 787:181–188